Sodium lidar measurements of mesopause region temperatures at 23° S

Barclay Clemesha *, Dale Simonich, Paulo Batista

Instituto Nacional de Pesquisas Espaciais, São José dos Campos, SP, Brazil

Received 17 August 2010; received in revised form 23 November 2010; accepted 24 November 2010
Available online 30 November 2010

Abstract

A sodium lidar, capable of measuring temperature in the 80–100 km region, has been in operation at São José dos Campos (23° S, 46 W) since March 2007. Good quality data have been obtained for late autumn, winter and spring, but weather conditions make it extremely difficult to make measurements from mid-November to mid- February. We find the temperature structure to be strongly modulated by tides and gravity waves, but average profiles typically show a primary mesopause height close to 100 km with temperatures around 180 K, and a tendency for a secondary minimum of about 185 K to occur close to 90 km. Vertical temperature gradients greater than 50 K/km are sometimes seen even on profiles averaged over several hours. The strongest gradients are always positive and are frequently associated with strong gradients in sodium concentration. On the other hand, we frequently see rapid changes in the temperature profile, suggesting that models and non-local temperature measurements, as made by satellite radiometers, for example, are of little use in applications such as the analysis of gravity wave propagation seen in airglow images.
© 2010 COSPAR. Published by Elsevier Ltd. Open access under the Elsevier OA license.

Keywords: MLT; Upper atmosphere; Temperature; Lidar; Sodium

1. Introduction

Lidar measurements of atmospheric sodium were pioneered by a number of workers at the Radio Research Station, Slough (now the Rutherford Appleton Laboratory) in UK (Bowman et al., 1969; Gibson and Sandford, 1972). The same workers were also the first to measure temperature via determination of the Doppler broadening of the sodium D2 line (Gibson et al., 1979). The first accurate measurements of the mesopause region temperature profile appear to have been made by Fricke and von Zahn (1985) at Andoya, followed by She et al. (1990) at Colorado State University. Since that time temperature measurements have also been made using potassium instead of sodium (von Zahn and Hoffner, 1996) and the alternative technique of the iron-Boltzmann lidar has been implemented at polar latitudes by Gardner et al. (2001) and at Arecibo by Raizada and Tepley (2002).

2. Instrumentation

At INPE, São José dos Campos (23° S, 46° W), we have been making measurements of atmospheric sodium since 1972 and temperature in the 80–100 km region since early 2007. Our lidar transmitter generates the required 589 nm emission by mixing the 1064 and 1319 nm outputs from two pulsed NdYag lasers, seeded by diode-pumped CW NdYag oscillators, as shown in Fig. 1, a technique first used by Kawahara et al. (2002) in their Syowa lidar. Wavelength control is achieved by thermally tuning the seeders, the temperatures of which are controlled by thermoelectric heater/coolers, each of which is in a feedback loop with a temperature sensor. To measure atmospheric temperature we alternate the laser wavelength between the D2a peak and the crossover minimum between the D2a and D2b peaks by tuning the 1064 seeder, the 1319 laser being left at a fixed wavelength. Long-term drift in the laser frequencies is taken care of by making multiple scans through the D2 lines at the start of every data run and using the signal returned from the Na layer as a reference. We normally find the drift in wavelength to be negligible except when

---

* Corresponding author.
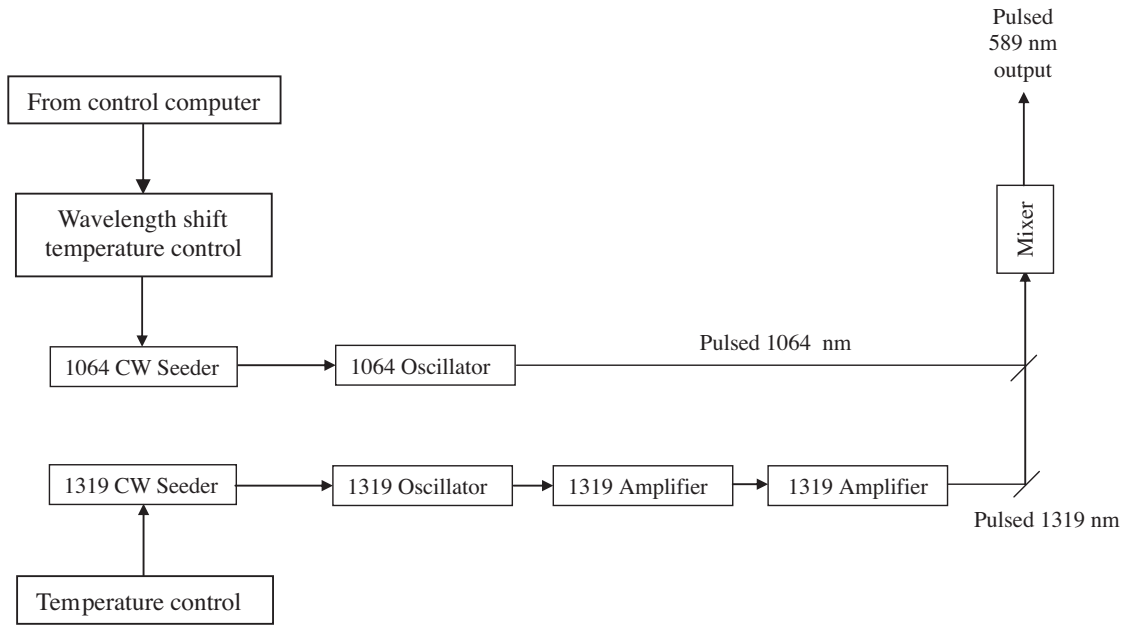 *E-mail address:* brc@laser.inpe.br (B. Clemesha).

Fig. 1. Narrow-band tunable pulsed laser for 589 nm.

the laser has been recently re-aligned. It is estimated that we can set the 589 nm output wavelength of the system to an accuracy of ±50 MHz. The thermal time constant of the seeders is such that it takes 40 s to switch wavelengths. We normally take 250 shots at the D2 peak followed by 750 at the crossover wavelength at 10 pps, so that a complete measurement cycle can be made in 3 min. Using high quantum efficiency Hamamatsu photomultipliers we typically count around 1000 pulses per 300 m height interval from the peak of the Na layer. We normally sum the signal over 5 height intervals in order to minimize the statistical fluctuations in the photon counts. The temperature is derived from the ratio of the relative Na scattering cross-sections at the two wavelengths, due allowance being made for the difference in the lidar beam extinctions. Variations in the transmission of the lower atmosphere and the laser pulse energy are taken into account by normalizing the lidar return to the Rayleigh scattering from 40 km. Variations in the sodium layer occurring between the on-line and off-line measurements are largely eliminated by interpolating the data at fixed times using a 3-point interpolation routine. This means that independent data points are 9 min apart and that only third order and above variations will affect the derived temperatures. In practice such variations are rare, even in the presence of sporadic layers. We estimate the absolute error in our temperature measurement in regions of high sodium concentration to be ±5 K. The absolute sodium concentration is determined by comparing the resonant scattering from the sodium layer with the Rayleigh scattering from around 40 km. We estimate the absolute accuracy of the measured sodium concentration to be about ±10%, and the relative error of the time/height – averaged profiles is about 2% at the peak of the layer. The ~100 MHz bandwidth of the laser emis-

sion, measured using a high finesse 2 GHz free spectral range Fabry Perot interferometer, is taken into account when computing temperatures. Our lidar configuration is somewhat unusual in that the basic lidar is aligned horizontally, aimed at a 120 cm flat mirror, making it possible to steer the beam over part of the sky. A simplified diagram of the laser optics is shown in Fig. 2 and relevant lidar parameters are given in Table 1.

3. Results

3.1. Mean temperature profile and seasonal variations

Local cloud cover makes it extremely difficult for us to operate the lidar in summer. As can be seen from Fig. 3, which shows the number of nights of data obtained per month since the start of operations in 2007, we have no data for January, three nights of data in December and 2 in November. We have reasonably good data coverage for the rest of the year. Note that all our measurements have been made at night. Nightly data runs are typically 8 h in duration so multiplying the ordinate scale of Fig. 3 by 8 gives the total data time in hours. The total amount of data analyzed in this paper amounts to about 1600 h, involving a total of about 9600 independent temperature profiles. The annual mean temperature profile is shown in Fig. 4. The profile shown in this figure is the mean of 11 monthly profiles, equal weight being given to each month. The error bars in Fig. 4, representing the standard deviations of the daily averages, give an idea of the geophysical noise in the data. The mean mesopause temperature is 180 K, just below 100 km, and there is a secondary mesopause at 89 km with a temperature of 185 K. The temperature rises rapidly above 100 km, reaching 200 K at
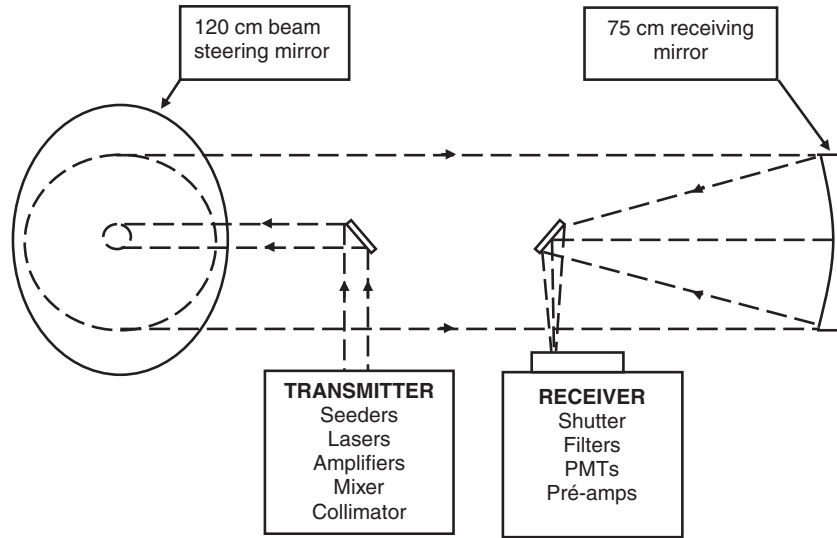
Fig. 2. Simplified optical layout of INPE lidar.

Table 1
INPE lidar parameters.

Location	23° S, 46° W
Wavelength	589 nm
Pulse energy	50 mJ
Pulse duration	20 nS
Pulse repetition rate	10 pps
Receiver telescope diameter	75 cm
Power aperture product	0.22 W, m^2
Height resolution	300 m (1.5 km for temperature)
Time resolution	3 min (9 min for temperature)

Fig. 4. Annual mean temperature profile for São José dos Campos. The error bars show the standard deviation of the daily means.
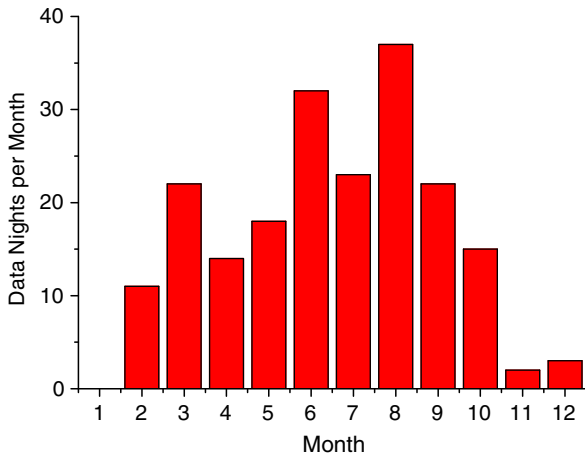

Fig. 3. Nights of data per calendar month, 2007–2010.

105 km. Lack of sodium prevents us from making temperature measurements above this height. The agreement with the CIRA annual mean standard atmosphere for 25° S is surprisingly good, except for the double mesopause which CIRA does not predict. Seasonal average profiles are shown in Fig. 5, from which it can be seen that autumn, winter and spring profiles are quite similar, with only the summer profile showing a major divergence from the
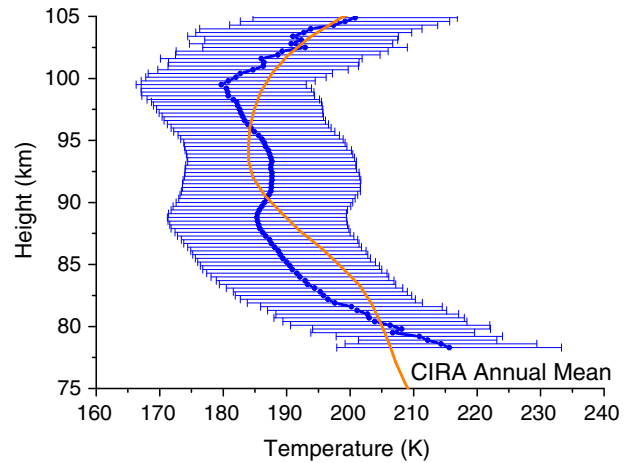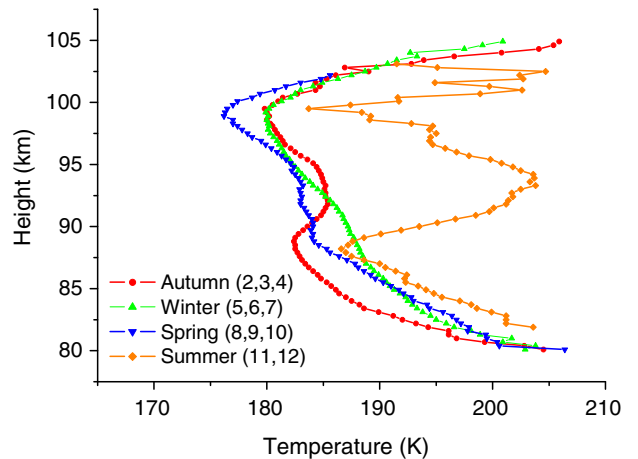

Fig. 5. Seasonal mean temperature profiles for São José dos Campos.

annual mean. The seasonal averages are based on month groupings (2, 3, 4), (5, 6, 7), (8, 9, 10) and (11, 12, 1) for autumn, winter, spring and summer, respectively. It must be remembered, of course, that the summer profile is based on only five nights of data and might not be altogether representative of the season. On the other hand, it should be pointed out that the five individual nightly profiles are quite similar, all showing a strong temperature inversion around 95 km. The seasonal variation of the temperature profile is shown in the form of a contour plot in Fig. 6. This figure shows the main mesopause at close to 100 km at all times of the year, but with colder temperatures at the equinoxes. The tendency for a double mesopause, with the secondary minimum about 10 km lower than the primary, is also more obvious at the equinoxes. Figs. 5 and 6 show that the temperature structure strongly diverges from the annual mean in the summer, with a temperature peak of over 200 K at 94 km. Also in summer, the temperatures of the primary and secondary mesopauses are about the same, whereas the 100 km mesopause is always colder during the rest of the year.

3.2. Vertical gradients in temperature and Na concentration

In an earlier paper (Clemesha et al., 2010) we showed that strong positive temperature gradients are related to strong gradients in sodium concentration. We also showed that positive temperature gradients are generally stronger than negative ones, despite the fact that the average temperature gradient is negative in the region in question (80–100 km). Here we present an analysis of a single night which shows a remarkable example of this behavior.

In Fig. 7 we show temperature and Na concentration profiles averaged over 9 min in time and 1.5 km in height for 2041 LT on November 3, 2009. Despite the height averaging, Fig. 7 shows a temperature increase of 75 K over a height interval of 1.8 km, indicating a temperature gradient of more than 40 K/km. We estimate the relative temperatures measured were accurate to approximately ±2.5 K.
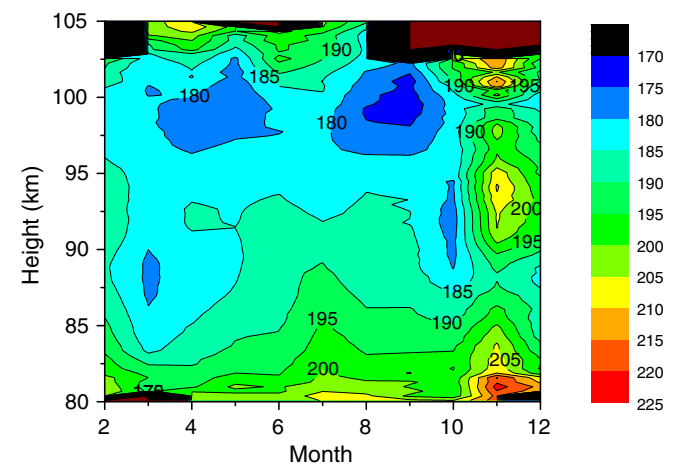
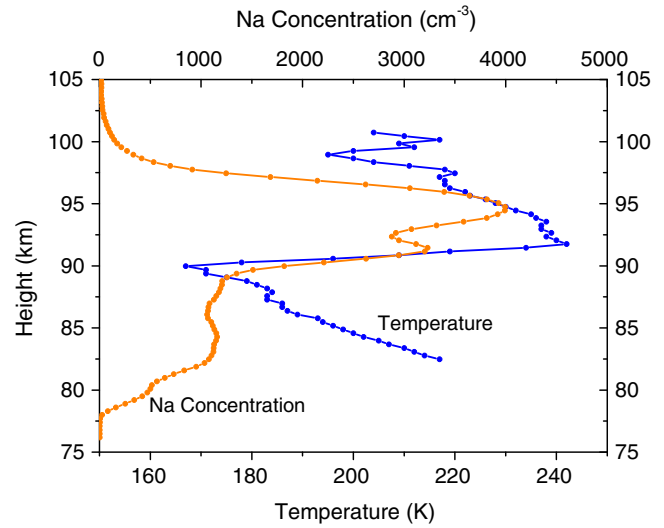Fig. 6. Contour plot showing seasonal temperature variation.

Fig. 7. Temperature and Na concentration profiles: 2041 LT, November 3, 2009.

If we deconvolve the temperature profile with the rectangular 1.5 km effective smoothing function applied by the height averaging, the gradient increases to 110 K/km. Even this value is probably an under-estimate since it does not take into account any variation in the profile over the 9 min time averaging period. At precisely the same height where this temperature transition takes place there occurs a very rapid increase in Na concentration. This relationship between the positive temperature gradient and the Na gradient continues throughout the night, as can be seen from the contour plots shown in Fig. 8. The coincidence between large positive temperature and Na concentration gradients can be seen even more clearly in Fig. 9, where we have plotted the vertical gradients in the two parameters. We can see from this figure that not only do the heights of the strong positive gradients in temperature and concentration correspond, but also their detailed vertical motions are almost identical. Fig. 9 also illustrates the fact that positive temperature gradients are much larger than negative ones. Although the behavior shown in Figs. 7–9 is an extreme example, closely correlated strong gradients in temperature and Na concentration are a common occurrence in our data, as is the predominance of large positive (as opposed to negative) temperature gradients. To show that this latter is the case we have calculated the occurrence frequency of vertical temperature gradients as a function of the gradient. The results of this analysis for all the data obtained during the year 2009 are shown in Fig. 10. The fact that this histogram is skewed towards high positive gradients makes it clear that the predominance of strong positive gradients is a regular characteristic of our measurements. This can be seen more clearly in Fig. 11, where we plot the ratio of positive to negative gradients as a function of the magnitude of the gradient. For small gradients negative values predominate, but for gradients greater than about 15 K/km the occurrence of positive gradients increases to an approximately asymptotic value of 2. In other words,
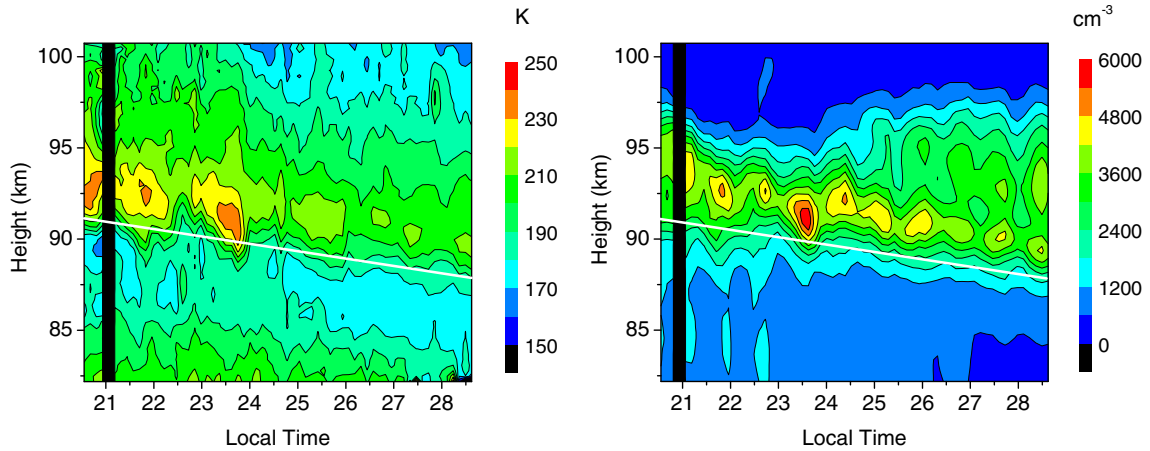
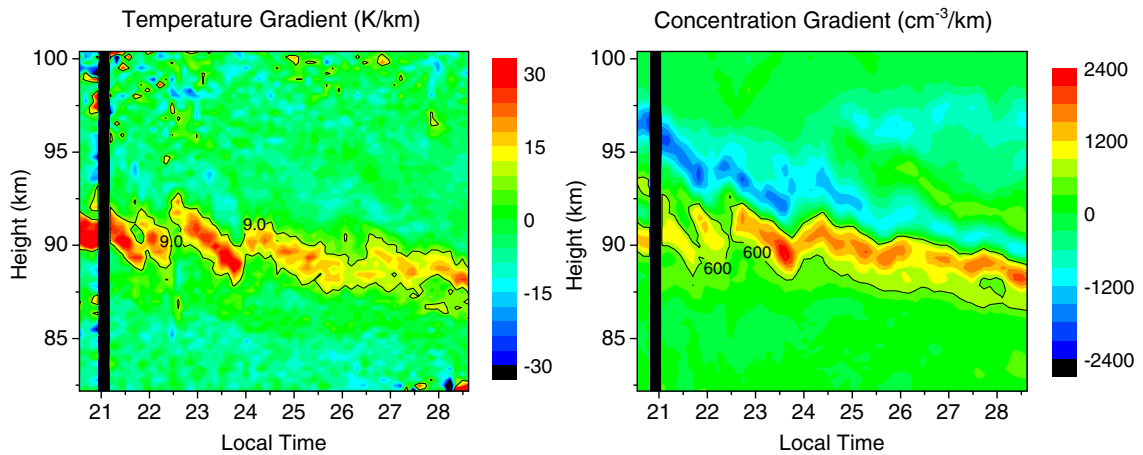Fig. 8. Temperature and Na concentration variations: November 3, 2009.

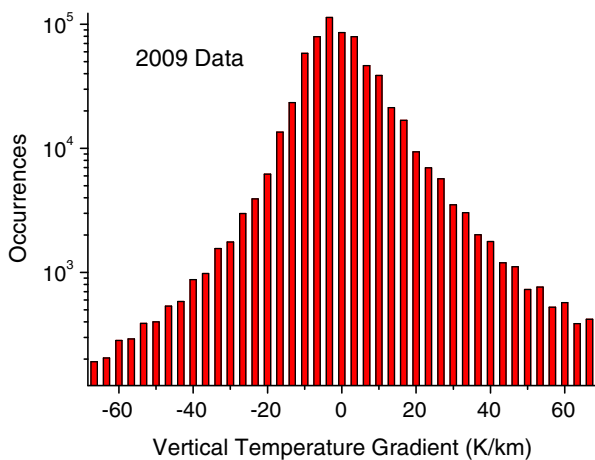Fig. 9. Vertical gradients of temperature and Na concentration: November 3, 2009.

Fig. 10. Gradient occurrence frequency – 2009 data.
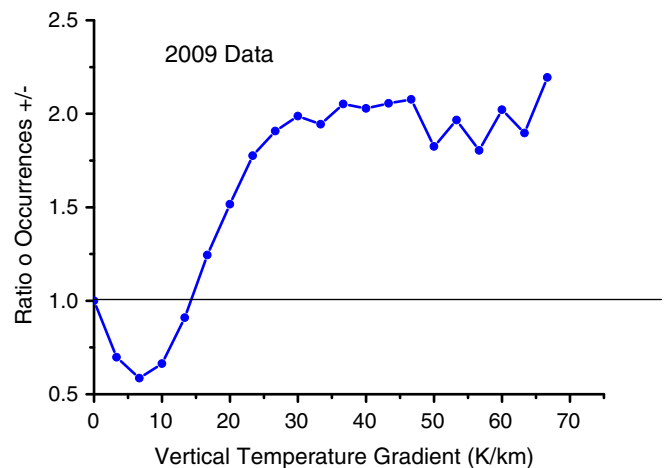
Fig. 11. Ratio of positive to negative gradient occurrence as a function of gradient magnitude.

strong positive gradients are about twice as likely to be encountered as strong negative ones.

With respect to our observation of large temperature gradients coincident with strong gradients in sodium concentration, it might be thought that the fact that our

on-line and off-line sodium measurements are made a few minutes apart could lead to false temperature gradients. This might happen in the presence of large and rapidly

changing sodium concentrations, as could occur in the region of a sporadic sodium layer, for example. There are a number of reasons to reject this possibility. Firstly, as explained earlier, we interpolate our concentration measurements at fixed coincident times with a second-order fit using three points at a time. This means that both linear and quadratic variations of Na concentration with time will be compensated by the interpolation process. Secondly, the coincident temperature and concentration gradients are often maintained for long periods of time, and thus involve quite slow temporal variations in Na concentration. In view of these considerations we can see no way in which the observed temperature gradient could be a measurement artifact.

4. Discussion

The annual mean temperature profile shown in Fig. 4 shows the same double mesopause feature as seen by Yu and She (1995) at 41° N. The main difference between our annual mean and that found by the Colorado State workers is that the temperatures at our 23° S site are nearly 10 K cooler than at their 41° N location. On the other hand, our temperatures are roughly consistent with the CIRA model, although the latter does not show the double mesopause feature.

Although small, the seasonal temperature variations shown in Figs. 5 and 6 are surprising. The existence of a cold summer mesopause for non-equatorial latitudes is well known, but our data show maximum temperatures in summer. Furthermore, we see temperature minima at the equinoxes, whereas most measurements at similar latitudes (Takahashi et al., 1994 – 23° S; Friedman and Chu, 2007 – 18° N; Gelinas et al., 2008 – 24° S) show equinox maxima. The observations made at Maui, Hawaii (21° N), by Chu et al. (2005) show little change in mesopause temperature between winter and equinoxes, only July showing a significantly lower and cooler mesopause than at other times of the year. It should be pointed out that the Hawaii observations (based on only six or seven nights of data for each season) do show a strong double mesopause in summer and, in this respect, they agree with ours. It must be admitted that that our summer maximum is based on only five nights of data, and thus may be atypical, but the equinox and winter profiles are based on many nights of measurement and it is difficult to see how the averages can be other than representative of their respective seasons. The main mesopause height is almost constant throughout the year at close to 100 km. This behavior is rather different to that seen at Arecibo (18° N – Friedman and Chu, 2007), where the summer mesopause is located close to 100 km, falling to about 96 km in winter. On the other hand, our observation of a persistent secondary mesopause at about 88 km is consistent with the two-level mesopause structure first suggested by Yu and She (1995). Our summer temperature maximum appears to result from strong heating, leading to a temperature inversion around

95 km. It is interesting to note that the strongest effect occurs in November, at which time of the year several other anomalies have been observed at our latitude. Clemesha et al. (1992) reported that the Na layer is about 1 km lower in November than at any other time of the year. Batista et al. (2004), observed a discontinuity in the phase of the diurnal tide in November at Cachoeira Paulista (23° S). It is possible that all these phenomena, heating in the 87–100 km range, decrease in height of the Na layer and discontinuity in the tidal phase could result from changes in the meridional circulation, leading to strong downwelling at this time of the year, with associated adiabatic heating. With respect to the secondary mesopause at around 90 km, however, it should be remembered that all our measurements have been made at night, so that the diurnal tide could influence our average vertical temperature profiles (see, for example, States and Gardner, 2000). The fairly short vertical wavelength seen by Batista et al. (2004) in the diurnal tidal wind at Cachoeira Paulista, about 100 km from our lidar site, is consistent with such an effect.

As mentioned above, we have commented on the existence of extremely strong vertical gradients in an earlier paper (Clemesha et al., 2010). These gradients, although they generally show downward vertical propagation, appear to be much stronger than would be expected from the perturbation due to a simple tide or gravity wave. The fact that positive temperature gradients (temperature increasing with height) are generally much stronger than negative ones, led us to suggest that they occur in regions of high atmospheric stability, where vertical eddy transport is inhibited. This suggestion is reinforced by the observation of large gradients in sodium concentration at the same height as the temperature gradients. Although the inhibition of eddy transport would help maintain strong positive temperature gradients (and both positive and negative gradients in sodium concentration) we are still unable to explain how gradients as high as 100 K/km form in the first place. It should be mentioned, here, that positive gradients of this magnitude have been seen at high latitudes by Fritts et al. (2004) who commented that they "occur in the context of an unusual summer mesopause circulation and structure", and ascribe their formation to "stronger than normal gravity wave forcing".

It is interesting to consider the implications of the temperature structure revealed by the lidar measurements. There is considerable interest in the role played by gravity waves in the MLT region. It is generally believed that waves generated in the troposphere propagate up to the mesopause region where they deposit energy and momentum with major effect on atmospheric structure. Several workers (Marks and Eckermann, 1995; Wrasse et al., 2006) have used reverse ray-tracing to estimate the possible origin of gravity waves seen on airglow imagers. This ray tracing requires a knowledge of the temperature structure and winds in the region through which the gravity waves are propagating. Such studies have invariably used models such as MSIS and/or reanalysis to model these parameters.

The large and rapid temperature variations revealed by height and time resolved lidar measurements such as ours suggest that the instantaneous temperature structure of the MLT, needed for realistic ray-tracing, bears little relationship to model outputs, the use of which will lead to unrealistic results from the ray-tracing process. It should also be remembered, of course, that reverse ray tracing reveals only the *possible* origin of gravity waves which might, in fact, originate at any point on the calculated ray trajectory.

5. Conclusions

Na resonance lidar measurements of the temperature from 80 to 105 km at 23° S show an annual mean profile with a double mesopause minimum. The main mesopause shows a temperature of 180 K at 100 km, and the secondary mesopause temperature is 185 K at 89 km.

The seasonal variation in the temperature of the main mesopause shows minima at the equinoxes and a maximum in summer. The summer maximum is the mean of only five nights of measurement and results from the existence of a strong temperature inversion on all these nights. For this reason it might not be typical of our location.

The secondary mesopause at around 85 km is present at all times of the year, although it is more pronounced in autumn and summer, becoming little more than an inflexion in the temperature profile in spring and winter. Since our measurements are made only during nighttime, it is possible that the secondary mesopause is related to the diurnal tide.

Strong positive temperature gradients up to 100 K/km are seen to persist from a few minutes up to 8 h. Long-lived gradients normally show downward propagation. Negative temperature gradients are always much less pronounced than the positive ones. Strong gradients in sodium concentration are frequently seen to coincide in height with the positive temperature gradients.

References

Batista, P.P., Clemesha, B.R., Tokumoto, A.S., Lima, L.M. Structure of the mean winds and tides in the meteor region over Cachoeira Paulista, Brazil (22.7 S, 45 W). J. Atmos. Solar Terr. Phys. 66, 623–636, 2004.

Bowman, M.R., Gibson, A.J., Sandford, M.C.W. Atmospheric sodium measured by a tuned laser radar. Nature 221, 456–457, 1969.

Gibson, A.J., Sandford, M.C.W. Daytime laser radar measurements of the atmospheric sodium layer. Nature 239, 509–511, 1972.

Chu, X., Gardner, C.S., Franke, S.J. Nocturnal thermal structure of the mesosphere and lower thermosphere region at Maui, Hawaii (20. N), and Starfire Optical Range, New Mexico (3 N). J. Geophys. Res. 110, doi:10.1029/2004JD004891, 2005.

Clemesha, B.R., Simonich, D.M., Batista, P.P. Mesopause region temperature structure observed by sodium resonance lidar. J. Atmos. Solar Terr. Phys., doi:10.1016/j.jastp.2010.03.017, 2010.

Clemesha, B.R., Simonich, D.M., Takahashi, H., Batista, P.P., Sahai, Y. The annual variation of the height of the atmospheric sodium layer at 23oS: Evidence for convective transport. J. Geophys. Res. 97, 5981–5986, 1992.

Friedman, J.S., Chu, X. Nocturnal temperature structure in the mesopause region over the Arecibo Observatory (18.35 N, 66.75 W): Seasonal variations. J. Geophys. Res. 112, doi:10.1029/2006JD008220, 2007.

Fritts, D.C., Williams, B.P., She, C.Y., Vance, J.D., Rapp, M., Lübken, F.-J., Müllemann, A., Schmidlin, F.J., Goldberg, R.A. Observations of extreme temperature and wind gradients near the summer mesopause during the MaCWAVE/MIDAS rocket campaign. Geophys. Res. Lett. 31 (24), L24S06, doi:10.1029/2003GL019389, 2004.

Fricke, K.H., Von Zahn, U. Mesopause temperatures derived from probing the hyperfine structure of the D2 resonance line of sodium by lidar. J. Atmos. Terr. Phys. 47, 499, 1985.

Gardner, C.S., Papan, G.C., Chu, X., Pan, W. First lidar observations of middle atmosphere temperatures, Fe densities and polar mesospheric clouds over the North and South Poles. Geophs. Res. Lett. 28, 1199–1202, 2001.

Gelinas, L.J., Hecht, J.H., Walterscheid, R.L., Roble, R.G., Woithe, J.M. A seasonal study of mesospheric temperatures and emission intensities at Adelaide and Alice Springs. J. Geophy. Res. 113, doi:10.1029/2007JA012587, 2008.

Gibson, A.J., Thomas, L., Bhattachacharyya, S.K. Laser observations of the ground-state hyperfine structure of sodium and of temperatures in the upper atmosphere. Nature 281, 131–132, 1979.

Kawahara, T.D., Kitahara, T., Kobayashi, F., Saito, Y., Nomura, A., She, C.-Y., Krueger, D.A., Tsutsumi, M. Wintertime mesopause temperatures observed by lidar measurements over Syowa station 69°S, 39°E, Antarctica. Geophys. Res. Lett. 29, doi:10.1029/2002GL015244, 2002.

Marks, C.J., Eckermann, S.D. A three-dimensional non-hydrostatic ray-tracing model for gravity waves: formulation and preliminary results for the middle atmosphere. J. Atmos. Sci. 52, 1959–1984, 1995.

Raizada, S., Tepley, C.A. Iron Boltzmann lidar temperature and density observations from Arecibo – An initial comparison with other techniques. Geophys. Res. Lett. 29, doi:10.1029/2001GL014535, 2002.

She, C.Y., Latifi, H., Yu, J.R., Alvarez, R.J., Bills, R.E., Gardner, C.S. Two-frequency lidar technique for mesospheric Na temperature measurements. Geophys. Res. Lett. 17, 929–932, 1990.

States, R.J., Gardner, C.S. Thermal structure of the mesopause region (80–105 km) at 408° N latitude. Part II: diurnal variations. J. Atmos. Sci. 57, 78–92, 2000.

Takahashi, H., Clemesha, B.R., Sahai, Y., Batista, P.P. Seasonal variations of the mesopause temperature observed at equatorial (4S) and low (23S) latitude stations. Adv. Space Res. 14 (9), 97–100, 1994.

Von Zahn, U., Hoffner, J. Mesopause temperature profiling by potassium lidar. Geophys. Res. Lett. 23 (2), 141–144, 1996.

Wrasse, C.M., Nakamura, T., Tsuda, T., Takahashi, H., Medeiros, A.F., Taylor, M.J., Gobbi, D., Salatun, A., Suratno, Achmad, E., Admiranto, A.G. Reverse ray tracing of the mesospheric gravity waves observed at 23°S (Brazil) and 7°S (Indonesia) in airglow imagers. J. Atmos. Solar Terr. Phys. 68 (2), 163–181, 2006.

Yu, J.R., She, C.Y. Climatology of a midlatitude mesopause region observed by a lidar at Fort Collins, Colorado (40.6N, 105W). J. Geophys. Res. 100 (D4), 7441–7452, 1995.